Optica Applicata, Vol. LIII, No. 1, 2023
DOI: 10.37190/oa230105

Monte Carlo simulation of polarization of light back-scattered from randomly rough surfaces

YUXIANG JIANG[1, 2,*], ZHENHUA LI[1,**]

[1]College of Science, Nanjing University of Science and Technology, Nanjing 210094, China

[2]Engineering Training Centre, Nanjing University of Science and Technology, Nanjing 210094, China

[*]Corresponding author: jiangyuxiang@njust.edu.cn

[**]Corresponding author: lizhenhua@njust.edu.cn

Laser detection devices obtain target information from back-scattered light, such as lidar. The recognition rate can be improved by analyzing intensity and polarization of echo signal. In this paper, Monte Carlo method is used to generate a large number of randomly rough surfaces to simulate targets. Every rough surface is discretized into a large number of micro-surface elements. Stokes parameters of back-scattered light are calculated by numerical integration. Incident light is p-, s-, 45° linearly polarized light and right-hand circularly polarized light, respectively. Numerical results show that when s- and p-linearly polarized light incident on a metal rough surface, back-scattered light appears circularly polarized component. Metal rough surface resembles a wave plate with phase difference, with the fast axis parallel or perpendicular to the 45° direction. When linearly polarized light is incident on dielectric rough surface, back-scattered light has no circularly polarized component. Experimental data are consistent with the numerical results. The above research provides a new basis for laser detection device to identify metal targets from the environmental background.

Keywords: back scattering, randomly rough surface, Stokes parameters, Monte Carlo method, polarized light.

1. Introduction

Lidar is a typical single-station detection system that detects position and velocity of a target by transmitting and receiving laser beam. Lidar detection can obtain very high resolution of angle, range, and speed, which has the advantages of good concealment and strong anti-active jamming ability. A laser beam has a good direction, and can be modulated very narrowly. It is very difficult for the enemy to intercept it. The transmitting system of lidar has small aperture and narrow receiving area, and the proba-

bility of laser jamming signal entering the receiver is very low. Therefore, lidar is suitable for working in an increasingly complex and intense information warfare environment. Due to the influence of various ground objects echo in a microwave radar, there are some blind areas in the low altitude. However, for lidar, only the irradiated target can produce reflection, and there is no impact of ground object echo at all. Therefore, it can work with good detection performance at low altitude. Lidar also has the advantages of small size and light weight. Traditional lidar only depends on the intensity of back-scattered light, which has great limitation. Polarization is an important property of laser and can effectively improve the information dimensions of echo. The polarization of the back-scattered light is closely related to the roughness, geometry, material and structure of the object surface. Which is taken into account in polarized lidar can greatly improve the detection performance.

Polarized lidar is based on the polarization property of back-scattered light. Prototype lidar development is complex and expensive. For the design of lidar, modeling and simulation of the polarization property of back-scattered light are very important. Numerical simulation technology has the characteristics of high accuracy and is easy to be carried out, which can provide a theoretical basis for the design of lidar prototype. Many scholars have studied the numerical analysis of the polarization characteristics of scattered light. SÁNCHEZ-GIL *et al*. numerically studied multiple scattering of light from one-dimensional randomly rough metallic surfaces by Monte Carlo simulation method based on the extinction-theorem boundary conditions [1,2]. MÉNDEZ *et al*. studied the statistics of the polarization properties of one-dimensional randomly rough surfaces [3]. MAKSIMOVA *et al*. studied the polarization characteristics of scattered light by the Monte Carlo computer simulation technique [4–6]. WANG *et al*. presented a full discussion on polarized light propagation in turbid media, and simulated the propagation behavior of two-dimensional Stokes vectors and Mueller matrices under various conditions by Monte Carlo algorithm [7]. JIN *et al*. showed the angle-resolved Stokes parameters of several objects with rough surface, and derived depolarized components caused by scattering [8]. They investigated the patterns of polarization degrees and the Stokes vectors of the scattered light in terms of transverse and longitudinal scattering angles [9]. DELACRÉTAZ *et al*. simulated the field back-scattered from a rough surface, and took into account polarization and multiple scattering events on the surface, as well as diffraction effects. They demonstrated the validity and usefulness of the simulation in the case of surface topology measurement [10]. LETNES *et al*. calculated the Mueller matrix, which contained all the polarization properties of light scattered from a two-dimensional randomly rough lossy metal surface [11,12]. GUIRADO *et al*. modeled reflection of light on rough surface by the Monte Carlo technique and found high sensitivity of the maximum of the degree of linear polarization to the real part of the refractive index [13]. They developed an accurate Monte Carlo method to predict polarization signatures of sunlight reflected from the surface of a planetary body [14]. WANG *et al*. proposed a novel Monte Carlo model to acquire the reflective polarization information from rough surface with arbitrary layers and profiles [15]. GUAN *et al*. simulated the

transmission characteristics of polarized light in water with specific particle and attenuation coefficient by the Monte Carlo program [16]. YUN *et al*. simulated polarized photon scattering in anisotropic media and tissues [17,18]. JIANG *et al*. described the depolarization characteristics of rough surface by M11/M00 of Mueller matrix [19,20]. YAN *et al*. calculates the Mueller matrix distribution of one- and two-dimensional rough surfaces [21–24]. The Monte Carlo simulations for polarization information reflection and transmission have made important progress. WANG *et al*. constructed an active imaging model within 10 km of the atmosphere from the satellite to the ground based on the Monte Carlo algorithm [25]. LI *et al*. described the glucose concentrations changes in the scattering system by polarization imaging technology [26]. They used indices of polarimetric purity obtained from different reflective interfaces as a criterion of depolarization property to characterize and classify targets covered by organic paint layers with different roughness [27]. They introduced a reflective polarization based computational ghost imaging system based on a Monte Carlo model under the foggy environments [28]. They proposed polarization remote sensing with the modified U-Net based deep-learning network [29], *etc*.

In the scattering calculation, the numerical simulation of the polarization property of back-scattered light used in lidar design is rare. It is important to carry out numerical simulation of scattered light polarization for lidar target detection and recognition. It can provide basis for lidar prototype development. In this paper, the Monte

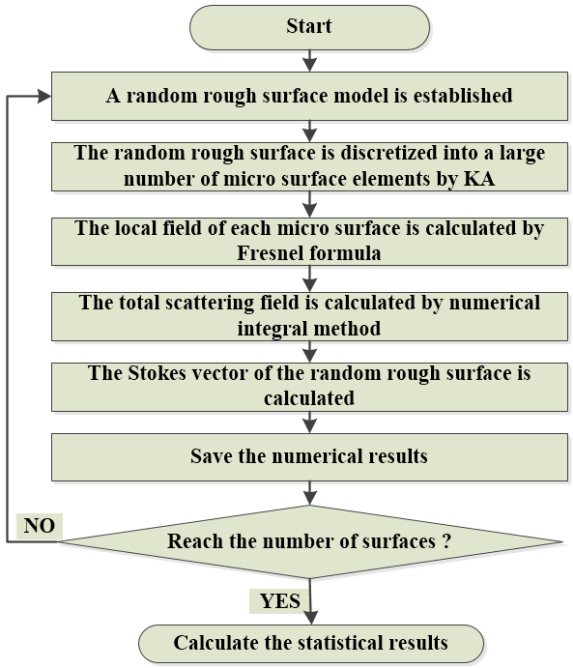

Fig. 1. The flowchart of Stokes vector calculation of back-scattered light by the Monte Carlo method.

Carlo method is used to generate a large number of randomly rough surfaces to simulate targets, and the flowchart of Stokes vector calculation of back-scattered light by the Monte Carlo method is shown in Fig. 1. Every rough surface is discrete into a large number of micro-surface elements. Kirchhoff approximation (KA) method is used to calculate the surface current and magnetic flux of the target surface, and then total scattering field is obtained. Back-scattered light of dielectric and metal rough surface is simulated numerically and obvious difference is found. Experimental measurements are carried out. It can provide a basis for the design of single-station laser detection system.

2. Methods

2.1. Generation of two-dimensional randomly rough surfaces

In practical application, it is necessary to measure the surface height fluctuation f_i ($i = 1, 2, ..., N$, and N is the number of sampling points). The length of the rough surface is L. Then, we can calculate the root mean square of rough surface height δ and the correlation coefficient $\rho(l)$:

$$\delta = \sqrt{\frac{1}{N-1}\left[\sum_{i=1}^{N} f_i^2 - N \cdot (\bar{f})^2 f\right]}, \quad \left(\bar{f} = \frac{1}{N}\sum_{i=1}^{N} f_i\right) \tag{1}$$

$$\rho(l) = \left[\sum_{i=1}^{N+1-j} f_i f_{i+j-1}\right]\left[\sum_{i=1}^{N} f_i^2\right]^{-1}, \quad (j = 1, 2, ..., N) \tag{2}$$

In Eq. (2), $l = (j-1)L/N$. When $\rho(l) = 1/e$, $l_c = l$, and l_c is called the correlation length.

TOPORKV *et al*. introduced a generation method of spectral fast Fourier transform (FFT) of one-dimensional randomly rough surface [30,31]. We introduced the generation of a two-dimensional rough surface.

The length and width of the two-dimensional rough surface are L_x and L_y. The sampling intervals are Δx and Δy, respectively. $\Delta x < 0.1\lambda$, $\Delta y < 0.1\lambda$ (and λ is the wavelength of incident light).

The sampling points $M = L_x/(2\Delta x)$, $N = L_y/(2\Delta y)$. An independent Gaussian random number matrix $r_{mn}(m = 0...2M, n = 0...2N)$ and $w_{mn}(m = 0...2M, n = 0...2N)$ that obey the standard normal distribution are generated. We combine them into complex random numbers:

$$\begin{cases} \hat{r}_{m0} = \dfrac{1}{2} r_{m0}, & (m = 0...2M) \\ \hat{r}_{0n} = \dfrac{1}{2} r_{0n}, & (n = 0...2N) \\ \hat{r}_{mn} = r_{mn} + i w_{mn}, & (m = 1...2M, n = 1...2N) \end{cases} \tag{3}$$

We calculate the expansion coefficient $\hat{\eta}_{mn}$

$$\begin{cases} \chi_{mn} = W\left(m\dfrac{2\pi}{L_x}, n\dfrac{2\pi}{L_y}\right), & (m = 0...M, n = 0...N) \\ \chi_{(2M-m)(2N-n)} = \chi_{m(2N-n)} = \chi_{(2M-m)n} = \chi_{mn} \\ \hat{\eta}_{mn} = \pi\sqrt{\dfrac{\chi_{mn}}{L_x L_y}}\,\hat{r}_{mn} \end{cases} \tag{4}$$

A two-dimensional FFT calculation is carried out

$$\hat{f}_{pq} = \sum_{m=0}^{2M}\sum_{n=0}^{2N}\hat{\eta}_{mn}\exp\left[i\left(\frac{2\pi}{M}pm + \frac{2\pi}{N}qn\right)\right] \tag{5}$$

We can obtain the highly discrete distribution of two-dimensional random rough surface f_{pq}

$$f_{pq} = 2\mathrm{Re}\{\hat{f}_{pq}\}, \quad (p = 0...2M, q = 0...2N) \tag{6}$$

The above derivation is applicable to any power spectral density function. We use the surface power spectral density function $W(K_x, K_y)$for calculation. The two-dimensional Gaussian power spectral density function is

$$W(K_x, K_y) = \delta^2\frac{l_x l_y}{4\pi}\exp\left(-\frac{K_x^2 l_x^2 + K_y^2 l_y^2}{4}\right) \tag{7}$$

The methods of FFT2D and IFFT2D are the core of rough surface modeling [32]. Constrained by computational complexity, rapid modeling of rough surfaces is required for Monte Carlo calculations. We set the height RMS of the rough surface δ is 0.4 μm, and the correlation length l_c is 4 μm. For example, the two-dimensional Gaussian randomly rough surface is generated by frequency filtering, as shown in Fig. 2.

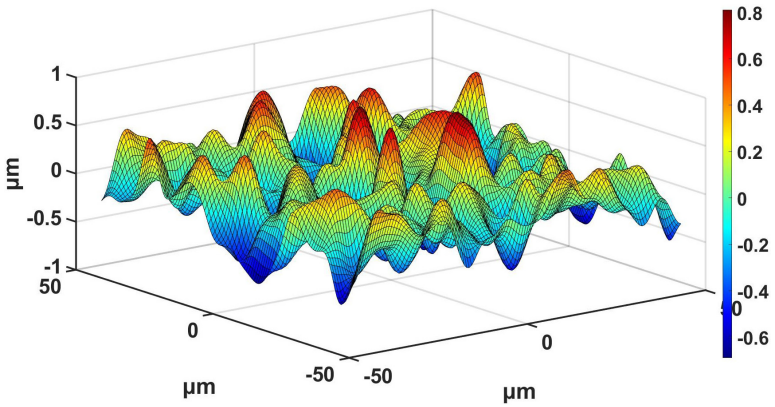

Fig. 2. Two-dimensional Gaussian randomly rough surface.

2.2. Calculation of the local field by Kirchhoff approximation

The electric and magnetic fields of incident light are [33]:

$$\begin{cases} \mathbf{E}_{\mathrm{i}} = E_0 \exp(-i k_0 \hat{\mathbf{k}}_{\mathrm{i}} \cdot \mathbf{r}') = (E_{\mathrm{v}}^{i} \hat{\mathbf{v}}_{\mathrm{i}} + E_{\mathrm{h}}^{i} \hat{\mathbf{h}}_{\mathrm{i}}) \exp(-i k_0 \hat{\mathbf{k}}_{\mathrm{i}} \cdot \mathbf{r}') \\ \mathbf{H}_{\mathrm{i}} = \dfrac{1}{\eta_0} \hat{\mathbf{k}}_{\mathrm{i}} \times \mathbf{E}_{\mathrm{i}} = \dfrac{1}{\eta_0} (E_{\mathrm{v}}^{i} \hat{\mathbf{h}}_{\mathrm{i}} - E_{\mathrm{h}}^{i} \hat{\mathbf{v}}_{\mathrm{i}}) \exp(-i k_0 \hat{\mathbf{k}}_{\mathrm{i}} \cdot \mathbf{r}') \end{cases} \tag{8}$$

In Eq. (8), $E_{\mathrm{v}}^{i} = E_0 \hat{\mathbf{v}}_i$, $E_{\mathrm{h}}^{i} = E_0 \hat{\mathbf{h}}_i$, and $\mathbf{r}'$ is position vector of a point on a randomly rough surface. Unit vector of incident light direction $\hat{\mathbf{k}}_{\mathrm{i}}$ and unit vector of the observed direction of scattered light $\hat{\mathbf{k}}_{\mathrm{s}}$ are:

$$\begin{cases} \hat{\mathbf{k}}_{\mathrm{i}} = \hat{\mathbf{x}} \sin\theta_{\mathrm{i}} \cos\varphi_{\mathrm{i}} + \hat{\mathbf{y}} \sin\theta_{\mathrm{i}} \sin\varphi_{\mathrm{i}} - \hat{\mathbf{z}} \cos\theta_{\mathrm{i}} \\ \hat{\mathbf{k}}_{\mathrm{s}} = \hat{\mathbf{x}} \sin\theta_{\mathrm{s}} \cos\varphi_{\mathrm{s}} + \hat{\mathbf{y}} \sin\theta_{\mathrm{s}} \sin\varphi_{\mathrm{s}} + \hat{\mathbf{z}} \cos\theta_{\mathrm{s}} \end{cases} \tag{9}$$

The vertically and parallel polarized unit vectors of incident plane are:

$$\begin{cases} \hat{\mathbf{h}}_{\mathrm{i}} = \dfrac{\hat{z} \times \hat{\mathbf{k}}_{\mathrm{i}}}{|\hat{z} \times \hat{\mathbf{k}}_{\mathrm{i}}|} = -\hat{\mathbf{x}} \sin\varphi_{\mathrm{i}} + \hat{\mathbf{y}} \cos\varphi_{\mathrm{i}} \\ \hat{\mathbf{v}}_{\mathrm{i}} = \hat{\mathbf{h}}_{\mathrm{i}} \times \hat{\mathbf{k}}_{\mathrm{i}} = -\hat{\mathbf{x}} \cos\theta_{\mathrm{i}} \cos\varphi_{\mathrm{i}} - \hat{\mathbf{y}} \cos\theta_{\mathrm{i}} \cos\varphi_{\mathrm{i}} - \hat{\mathbf{z}} \sin\theta_{\mathrm{i}} \end{cases} \tag{10}$$

The vertically and parallel polarized unit vectors of scattered plane are:

$$\begin{cases} \hat{\mathbf{h}}_{\mathrm{s}} = \dfrac{\hat{z} \times \hat{\mathbf{k}}_{\mathrm{s}}}{|\hat{z} \times \hat{\mathbf{k}}_{\mathrm{s}}|} = -\hat{\mathbf{x}} \sin\varphi_{\mathrm{s}} + \hat{\mathbf{y}} \cos\varphi_{\mathrm{s}} \\ \hat{\mathbf{v}}_{\mathrm{s}} = \hat{\mathbf{h}}_{\mathrm{s}} \times \hat{\mathbf{k}}_{\mathrm{s}} = \hat{\mathbf{x}} \cos\theta_{\mathrm{s}} \cos\varphi_{\mathrm{s}} + \hat{\mathbf{y}} \cos\theta_{\mathrm{s}} \cos\varphi_{\mathrm{s}} - \hat{\mathbf{z}} \sin\theta_{\mathrm{s}} \end{cases} \tag{11}$$

We set $\theta_{\mathrm{i}} = \theta_{\mathrm{s}}$, $\varphi_{\mathrm{s}} = \pi - \varphi_{\mathrm{i}}$, and the back-scattering can be calculated. The back scattering diagram of randomly rough surface is shown in Fig. 3.

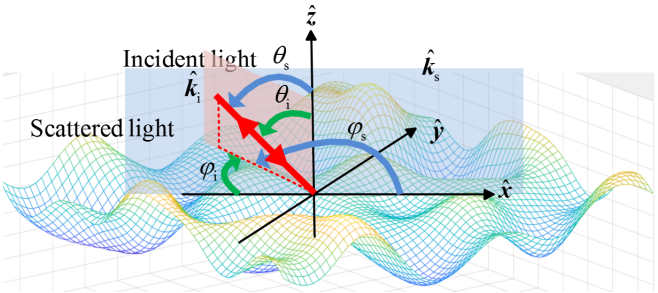

Fig. 3. The back scattering diagram of random rough surface.

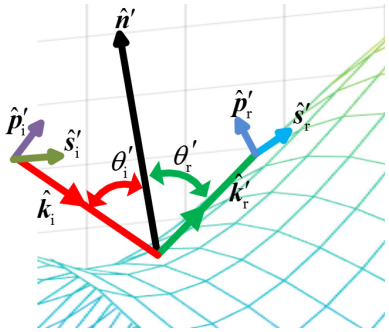

Fig. 4. The schematic diagram of local field calculation.

A randomly rough surface is discretized into a large number of tiny surface elements. The area of each surface element is $0.1\lambda \times 0.1\lambda$, and λ is the wavelength of incident light. The schematic diagram of local field calculation is shown in Fig. 4. The Fresnel formal is appropriate only in the circumstance that the interface is considerably larger than the incident wavelength. It is applicable only to plane calculation of reflection and refraction coefficients. For randomly rough surfaces, we use Kirchhoff tangent plane approximation. We discrete a complex rough surface into a large number of micro-elements. Each microplane is treated as a plane and the local reflection field is calculated using Fresnel formula. The Stratton–Chu integral equation is used to calculate the spatial scattering field. By calculating the space scattering field of a large number of randomly rough surfaces, the statistical stable value can be obtained.

A incident light can be resolved by the local polarization direction:

$$\begin{cases} \mathbf{E}'_i = (E^i_{v'}\hat{\mathbf{v}}'_i + E^i_{h'}\hat{\mathbf{h}}'_i)\exp(-ik_0\hat{\mathbf{k}}_i\cdot\mathbf{r}') \\ \mathbf{H}'_i = \dfrac{1}{\eta_0}(E^i_{v'}\hat{\mathbf{h}}'_i - E^i_{h'}\hat{\mathbf{v}}'_i)\exp(-ik_0\hat{\mathbf{k}}_i\cdot\mathbf{r}') \end{cases} \tag{12}$$

In Eq. (12), $E^i_{v'} = \mathbf{E}_i\cdot\hat{\mathbf{v}}'_i$ and $E^i_{h'} = \mathbf{E}_i\cdot\hat{\mathbf{h}}'_i$.

The vertically and parallel polarized unit vector of local incident plane is:

$$\begin{cases} \hat{\mathbf{h}}'_i = \dfrac{\hat{\mathbf{n}}'\times\hat{\mathbf{k}}_i}{|\hat{\mathbf{n}}'\times\hat{\mathbf{k}}_i|} \\ \hat{\mathbf{v}}'_i = \hat{\mathbf{h}}'\times\hat{\mathbf{k}}'_i \end{cases} \tag{13}$$

Unit normal vector of local surface element is:

$$\hat{\mathbf{n}}' = \frac{-z_x\hat{\mathbf{x}} - z_y\hat{\mathbf{y}} + \hat{\mathbf{z}}}{|1 + z_x^2 + z_y^2|} \tag{14}$$

In Eq. (14), $z_x = \partial z/\partial x$ and $z_y = \partial z/\partial y$. The height of the randomly rough surface is $z = z(x, y)$.

Each surface element can be viewed as a plane, and we calculate the local reflected field by Fresnel formula:

$$\begin{cases} \mathbf{E}'_{\mathrm{r}} = (r'_{\mathrm{v}} E^{\mathrm{i}}_{\mathrm{v}'} \hat{\mathbf{v}}'_{\mathrm{r}} + r'_{\mathrm{h}} E^{\mathrm{i}}_{\mathrm{h}'} \hat{\mathbf{h}}'_{\mathrm{r}}) \exp(-i k_0 \hat{\mathbf{k}}_{\mathrm{i}} \cdot \mathbf{r}') \\ \mathbf{H}'_{\mathrm{r}} = \dfrac{1}{\eta_0} (r'_{\mathrm{v}} E^{\mathrm{i}}_{\mathrm{v}'} \hat{\mathbf{h}}'_{\mathrm{r}} - r'_{\mathrm{h}} E^{\mathrm{i}}_{\mathrm{h}'} \hat{\mathbf{v}}'_{\mathrm{r}}) \exp(-i k_0 \hat{\mathbf{k}}_{\mathrm{i}} \cdot \mathbf{r}') \end{cases} \tag{15}$$

In Eq. (15), local reflection coefficients r'_{v} and r'_{h} are:

$$\begin{cases} r'_{\mathrm{v}} = \dfrac{n^2 \cos\theta'_{\mathrm{i}} - \sqrt{n^2 - \sin^2\theta'_{\mathrm{i}}}}{n^2 \cos\theta'_{\mathrm{i}} + \sqrt{n^2 - \sin^2\theta'_{\mathrm{i}}}} \\ r'_{\mathrm{h}} = \dfrac{\cos\theta'_{\mathrm{i}} - \sqrt{n^2 - \sin^2\theta'_{\mathrm{i}}}}{\cos\theta'_{\mathrm{i}} + \sqrt{n^2 - \sin^2\theta'_{\mathrm{i}}}} \end{cases} \tag{16}$$

In Eq. (16), the local incident angle is $\theta'_{\mathrm{i}} = \arccos(-\hat{\mathbf{n}}' \cdot \hat{\mathbf{k}}_{\mathrm{i}})$. The vertically and parallel polarized unit vectors of local reflection plane are:

$$\begin{cases} \hat{\mathbf{h}}'_{\mathrm{r}} = \dfrac{\hat{\mathbf{n}}' \times \hat{\mathbf{k}}_{\mathrm{r}}}{|\hat{\mathbf{n}}' \times \hat{\mathbf{k}}_{\mathrm{r}}|} \\ \hat{\mathbf{v}}'_{\mathrm{r}} = \hat{\mathbf{h}}'_{\mathrm{r}} \times \hat{\mathbf{k}}'_{\mathrm{r}} \end{cases} \tag{17}$$

In Eq. (17), $\hat{\mathbf{k}}'_{\mathrm{r}} = \hat{\mathbf{k}}_{\mathrm{i}} - 2(\hat{\mathbf{n}}' \cdot \hat{\mathbf{k}}_{\mathrm{i}})\hat{\mathbf{n}}'$.

The sum of the local incident field and the local reflection field is local field:

$$\begin{cases} \mathbf{E}' = \mathbf{E}'_{\mathrm{i}} + \mathbf{E}'_{\mathrm{r}} \\ \mathbf{H}' = \mathbf{H}'_{\mathrm{i}} + \mathbf{H}'_{\mathrm{r}} \end{cases} \tag{18}$$

2.3. Calculation of Mueller matrix and Stokes vector

The surface equivalent current $\mathbf{J}_{\mathrm{s}}$ and magnetic current $\mathbf{J}_{\mathrm{ms}}$ are:

$$\begin{cases} \mathbf{J}_{\mathrm{s}} = \int \hat{\mathbf{n}}' \times (\mathbf{H}'_{\mathrm{i}} + \mathbf{H}'_{\mathrm{r}}) \exp(-i k_0 \hat{\mathbf{k}}_{\mathrm{s}} \cdot \mathbf{r}') \sqrt{1 + z_x^2 + z_y^2}\, \mathrm{d}x\, \mathrm{d}y \\ \mathbf{J}_{\mathrm{ms}} = \int -\hat{\mathbf{n}}' \times (\mathbf{E}'_{\mathrm{i}} + \mathbf{E}'_{\mathrm{r}}) \exp(-i k_0 \hat{\mathbf{k}}_{\mathrm{s}} \cdot \mathbf{r}') \sqrt{1 + z_x^2 + z_y^2}\, \mathrm{d}x\, \mathrm{d}y \end{cases} \tag{19}$$

The scattering field is calculated according to the Stratton–Chu equation:

$$\mathbf{E}_{\mathrm{s}} = ik_0 \frac{\exp(-ik_0 R)}{4\pi R}(\eta_0 \mathbf{J}_{\mathrm{s}} - \hat{\mathbf{k}}_{\mathrm{s}} \times \mathbf{J}_{\mathrm{ms}}) \tag{20}$$

and $\mathbf{E}_{\mathrm{s}}$ can be divided into the vertical component E_{v} and the horizontal component E_{h}. We can calculate the Jones matrix J and its conjugate matrix J^*.

$$\begin{cases} \begin{bmatrix} E_{\mathrm{v}} \\ E_{\mathrm{h}} \end{bmatrix} = J \begin{bmatrix} E_{\mathrm{v}}^{\mathrm{i}} \\ E_{\mathrm{h}}^{\mathrm{i}} \end{bmatrix}, \quad J = \begin{bmatrix} j_{11} & j_{12} \\ j_{21} & j_{22} \end{bmatrix} \\ J^* = \begin{bmatrix} g_{11} & g_{12} \\ g_{21} & g_{22} \end{bmatrix} \end{cases} \tag{21}$$

where $E_{\mathrm{v}}^{\mathrm{i}}$, $E_{\mathrm{h}}^{\mathrm{i}}$ are the vertical and horizontal components of the incident electric field. We set $E_{\mathrm{v}}^{\mathrm{i}} = 1$ and $E_{\mathrm{h}}^{\mathrm{i}} = 0$, and can calculate the j_{11}, j_{21}. We set $E_{\mathrm{v}}^{\mathrm{i}} = 0$ and $E_{\mathrm{h}}^{\mathrm{i}} = 1$, and can calculate the j_{12}, j_{22}. And then we can compute the Mueller matrix according to the Jones matrix using Eq. (21), $\langle \cdot \rangle$ is the average.

$$\begin{cases} m_{11} = \langle g_{11}j_{11} + g_{21}j_{21} + g_{12}j_{12} + g_{22}j_{22} \rangle / 2 \\ m_{12} = \langle g_{11}j_{11} + g_{21}j_{21} - g_{12}j_{12} - g_{22}j_{22} \rangle / 2 \\ m_{13} = \langle g_{11}j_{12} + g_{21}j_{22} + g_{12}j_{11} + g_{22}j_{21} \rangle / 2 \\ m_{14} = \langle g_{11}j_{12} + g_{21}j_{22} - g_{12}j_{11} - g_{22}j_{21} \rangle / 2 \\ m_{21} = \langle g_{11}j_{11} + g_{12}j_{12} - g_{21}j_{21} - g_{22}j_{22} \rangle / 2 \\ m_{22} = \langle g_{11}j_{11} + g_{22}j_{22} - g_{12}j_{12} + g_{21}j_{21} \rangle / 2 \\ m_{23} = \langle g_{12}j_{11} + g_{11}j_{12} - g_{21}j_{22} - g_{21}j_{22} \rangle / 2 \\ m_{24} = i\langle g_{11}j_{12} + g_{22}j_{21} - g_{21}j_{22} - g_{12}j_{11} \rangle / 2 \\ m_{31} = \langle g_{11}j_{21} + g_{22}j_{11} + g_{12}j_{22} + g_{22}j_{12} \rangle / 2 \\ m_{32} = \langle g_{11}j_{21} + g_{21}j_{11} - g_{12}j_{22} - g_{22}j_{12} \rangle / 2 \\ m_{33} = \langle g_{11}j_{22} + g_{21}j_{12} + g_{12}j_{21} + g_{22}j_{11} \rangle / 2 \\ m_{34} = i\langle g_{11}j_{22} + g_{21}j_{12} - g_{12}j_{21} - g_{22}j_{11} \rangle / 2 \\ m_{41} = i\langle g_{21}j_{11} + g_{22}j_{12} - g_{11}j_{21} + g_{12}j_{22} \rangle / 2 \\ m_{42} = i\langle g_{21}j_{11} + g_{12}j_{22} - g_{11}j_{21} + g_{22}j_{12} \rangle / 2 \\ m_{43} = i\langle g_{21}j_{12} + g_{22}j_{11} - g_{11}j_{22} - g_{12}j_{21} \rangle / 2 \\ m_{44} = \langle g_{22}j_{11} + g_{11}j_{22} - g_{12}j_{21} + g_{21}j_{12} \rangle / 2 \end{cases} \tag{22}$$

The $\mathbf{S}_{in}$ and $\mathbf{S}_{out}$ are the Stokes vectors of the incident and scattered light. The $\mathbf{S}_{in}$ and $\mathbf{S}_{out}$ have the relationship:

$$\mathbf{S}_{out} = \mathbf{M}\,\mathbf{S}_{in} \tag{23}$$

$$\begin{bmatrix} \mathbf{I}_{out} \\ \mathbf{Q}_{out} \\ \mathbf{U}_{out} \\ \mathbf{V}_{out} \end{bmatrix} = \begin{bmatrix} m_{11} & m_{12} & m_{13} & m_{14} \\ m_{21} & m_{22} & m_{23} & m_{24} \\ m_{31} & m_{32} & m_{33} & m_{34} \\ m_{41} & m_{42} & m_{43} & m_{44} \end{bmatrix} \begin{bmatrix} \mathbf{I}_{in} \\ \mathbf{Q}_{in} \\ \mathbf{U}_{in} \\ \mathbf{V}_{in} \end{bmatrix} \tag{24}$$

The $\mathbf{M} = (m_{ij})_{1 \le ij \le 4}$ is a 4×4 matrix which characterizes the sample. The electric field which is only vibrating in the direction of $\hat{\mathbf{v}}$ is called p-linearly polarized light. And that which is only vibrating in the direction of $\hat{\mathbf{h}}$ is called s-linearly polarized light. The light with an angle of 45° between the direction of electric field vibration and the incident surface is called 45°-linearly polarized light. The Stokes vectors of p-, s-, 45°-polarized and right-handed circularly polarized light are $[1\ 1\ 0\ 0]^T$, $[1\ -1\ 0\ 0]^T$, $[1\ 0\ 1\ 0]^T$, $[1\ 0\ 0\ 1]^T$. We can calculate the Stokes vector of scattered light by Eq. (24). When only the case inside the incident plane is considered, the Mueller matrix can be reduced to the one-dimensional case:

$$\begin{bmatrix} \mathbf{I}_{out} \\ \mathbf{Q}_{out} \\ \mathbf{U}_{out} \\ \mathbf{V}_{out} \end{bmatrix} = \begin{bmatrix} \dfrac{|r_h|^2 + |r_v|^2}{2} & \dfrac{|r_h|^2 - |r_v|^2}{2} & 0 & 0 \\ \dfrac{|r_h|^2 - |r_v|^2}{2} & \dfrac{|r_h|^2 + |r_v|^2}{2} & 0 & 0 \\ 0 & 0 & -r_v r_h \cos\varphi & -r_v r_h \sin\varphi \\ 0 & 0 & r_v r_h \sin\varphi & -r_v r_h \cos\varphi \end{bmatrix} \begin{bmatrix} \mathbf{I}_{in} \\ \mathbf{Q}_{in} \\ \mathbf{U}_{in} \\ \mathbf{V}_{in} \end{bmatrix} \tag{25}$$

The reflectivities of dielectric and metal random rough surfaces are $r_v = |r_v|\exp(i\varphi_v)$ and $r_h = |r_h|\exp(i\varphi_h)$, and $\varphi = \varphi_v - \varphi_h$. In order to verify the effectiveness of the Monte Carlo method, we simulated some experimental and numerical results [34–37]. Compared with the simulation and experimental results in reference, a good consistency is obtained. The whole simulation is applying Matlab 2020a with computer based calculation platform (Intel i7, 3.40 GHz, 16G RAM). The calculations could be made faster using FORTRAN programming. However, the data interaction and display capabilities of FORTRAN were not good enough, so we chose MATLAB. We need to make full use of matrix techniques to avoid loops.

3. Numerical results

The wavelength of incident light $\lambda = 905$ nm is selected as the wavelength of lidar. The angle of scattering is $\theta_s \in [0°, 90°]$. Dielectric (glass) and metal (iron) are se-

lected as typical target materials. The refractive index of glass is 1.5 when λ = 905 nm, and the refractive index of iron is 3.12 + i3.87. The length and width of each randomly rough surface are 51.2λ. We set the correlation length $l_c = 6\lambda$. The surface roughness is characterized only by δ. $\delta = 0.1\lambda$, then the Stokes vector numerical simulation is carried out. p-, s-, 45°-linearly polarized light and right-hand circularly polarized light are selected as the four typical incident light. Five hundred Gaussian rough surfaces are generated to calculate, the calculation time is 12.5977 hour. In fact, the target material can be determined by V component of Stokes vector by calculating ten rough surfaces, and the calculation time is 15.1722 minutes. If we configure a better graphics card and use the Matlab GPU acceleration technology, the time will be shorter.

3.1. Stokes vector of back-scattered light of dielectric and metal rough surface

Figure 5 shows Stokes vector of back-scattered light of dielectric surface. The polarization of incident light has little effect on the intensity distribution of scattered light. According to reference [38], Fresnel reflection coefficients of p- and s-light are almost the same when the incident angle is small, $r_v \approx r_h$. Reflectivity $R_v = |r_v|^2$, $R_h = |r_h|^2$ and $R_v \approx R_h$. As the Fresnel reflection coefficients r_v, r_h of the dielectric rough surface are real numbers and there is no phase difference, the change in the polarization state of the scattered light is very small.

Figure 6 shows Stokes vector of back-scattered light of metal surface. The intensity of back-scattered light from metal rough surface is much greater than that from dielectric

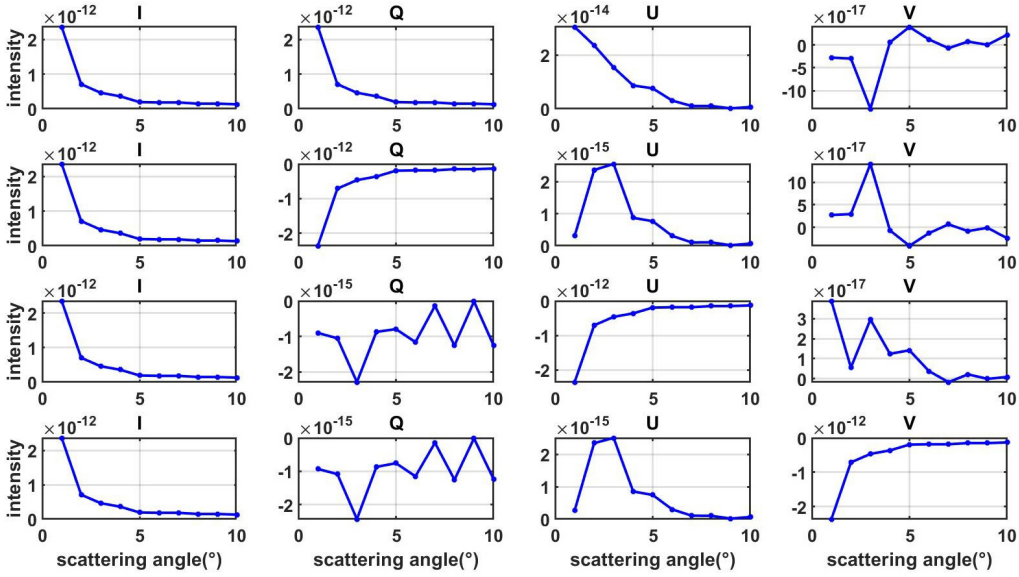

Fig. 5. Stokes vector of back-scattered light of dielectric surface (first row: p-light incident, second row: s-light incident, third row: 45° light incident, fourth row: right-hand circularly polarized light incident).

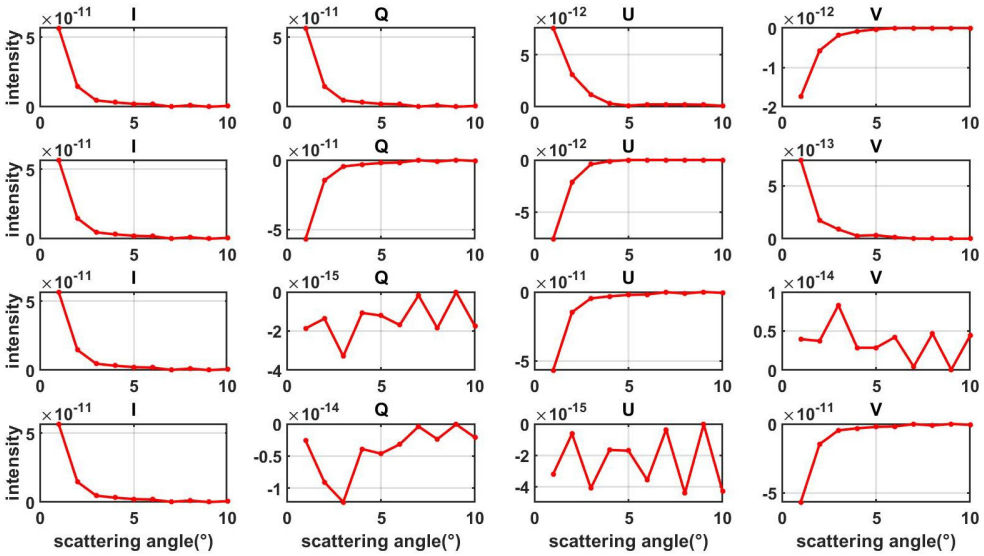

Fig. 6. Stokes vector of back-scattered light of metal surface (first row: p-light incident, second row: s-light incident, third row: 45° light incident, fourth row: right-hand circularly polarized light incident).

rough surface. According to reference [38], the reflectivity of metal rough surface is much greater than that of dielectric rough surface.

For the convenience of comparison, we normalized Stokes vectors respectively. Figure 7 shows distribution of normalized Stokes vector.

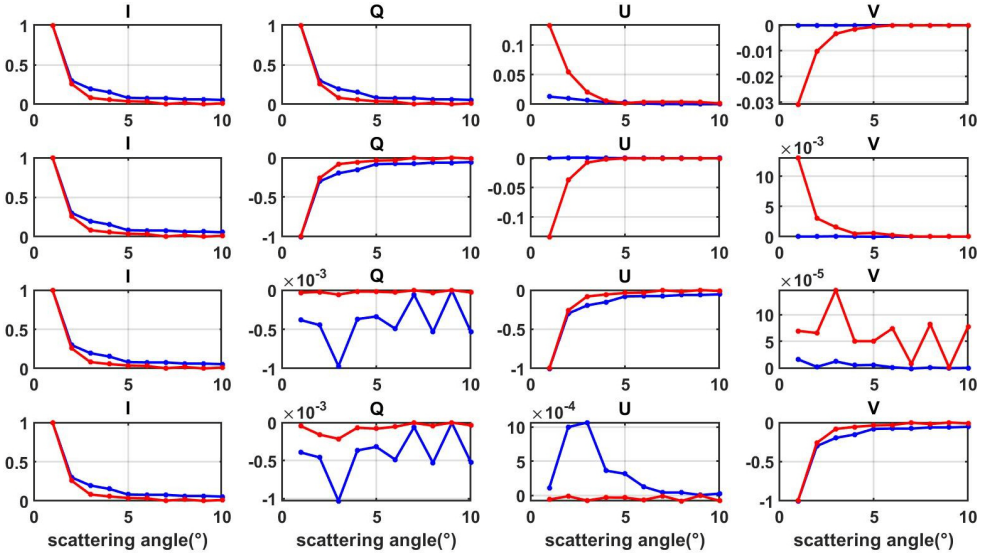

Fig. 7. Distribution of normalized Stokes vector (first row: p-light incident, second row: s-light incident, third row: 45° light incident, fourth row: right-hand circularly polarized light incident).

When p- and s-linearly polarized light is incident on the metal rough surface, scattered light has obvious circularly polarized component. When 45° linearly polarized light is incident on the rough surface of metal, the scattered light has no circularly polarized component. The metallic rough surface resembles a wave plate with phase delay. The fast axis of the wave plate is perpendicular or parallel to the 45° direction.

3.2. Scattering mechanism analysis

The reflection coefficients of dielectric and metal random rough surfaces are $r_h = |r_h|\exp(i\varphi_h)$ and $r_v = |r_v|\exp(i\varphi_v)$. In Eq. (25), $\varphi = \varphi_v - \varphi_h$, φ is only related to the material of the random rough surface. For linearly polarized light, $V_{in} = 0$. $V_{out} = U_{in} r_h r_v \sin\varphi$. Although the height fluctuation of the rough surface fluctuates randomly, the value of $r_h r_v \sin\varphi$ is stable. Since $r_h r_v \sin\varphi$ is always negative, the **V** and **U** have antisymmetric peak distributions. For dielectric randomly rough surface $\varphi = 0$ or π, however φ is not zero about metal randomly rough surface. The Stokes vector of p-, s- and 45°-linearly polarized light are $[1\ 1\ 0\ 0]^T$, $[1\ -1\ 0\ 0]^T$, and $[1\ 0\ 1\ 0]^T$. We know from Eq. (25) that $V_{out} \neq 0$ when p- and s-linearly polarized light is incident on the metal rough surface in the incident plane, and the rest of the other cases $V_{out} = 0$ in the incident plane. In practice, the Stokes vector **V** can be measured. It is concluded that using the linearly polarized light can distinguish the metallic and dielectric targets. It provides a new method for metal target recognition in laser detection system.

4. Experimental measurements

Experimental measurement is an important means to verify the scattering model. The Stokes vector of back-scattered light from metal and dielectric targets is measured in an experimental setup.

4.1. Experimental apparatus and measurement method

Figure 8 shows schematic diagram of experimental measuring device. A semiconductor laser with $\lambda = 905$ nm is selected. It can produce linearly polarized light with

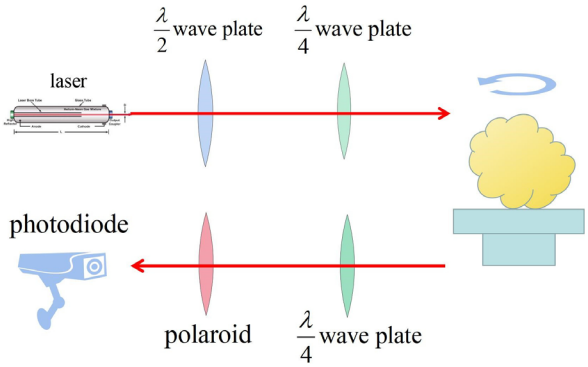

Fig. 8. Schematic diagram of experimental measuring device.

a polarization ratio of 100:1. The vibration direction of linearly polarized light can be changed by rotating the $\lambda/2$ wave plate. Circularly polarized light can be produced by rotating the fast axis of the $\lambda/4$ wave plate.

For the receiving circuit, the angle between the polarizer transmittance axis and $\hat{v}$ is α. The angle between the fast axis of the $\lambda/4$ wave plate and $\hat{v}$ is β. $I(\alpha, \Delta\varphi)$ represents the intensity of scattered light received by the detector. When $\beta = 0°$, we can get $I(0°, 0)$, $I(90°, 0)$, $I(45°, 0)$ and $I(45°, \pi/2)$, by rotating the polarizer [39]. When $\beta = 45°$ and $\alpha = 45°$, we can get $I(45°, 0)$.

The Stokes vector of back-scattered light can be obtained by the following formula:

$$\begin{cases} I = I(0°, 0) + I(90°, 0) \\ Q = I(0°, 0) - I(90°, 0) \\ U = 2I(45°, 0) - I \\ V = 2I(45°, \pi/2) - I \end{cases} \tag{26}$$

A glass is selected to represent the dielectric rough surface, $\delta = 0.289$ μm. A smooth iron sheet is selected to represent the rough metal surface, $\delta = 0.414$ μm.

4.2. Experimental results

4.2.1. Stokes vector of back-scattered light from randomly rough surface

Figures 9 and 10 show Stokes vectors of back-scattered light of dielectric and metal surface. Figure 11 shows the distribution of normalized Stokes vector.

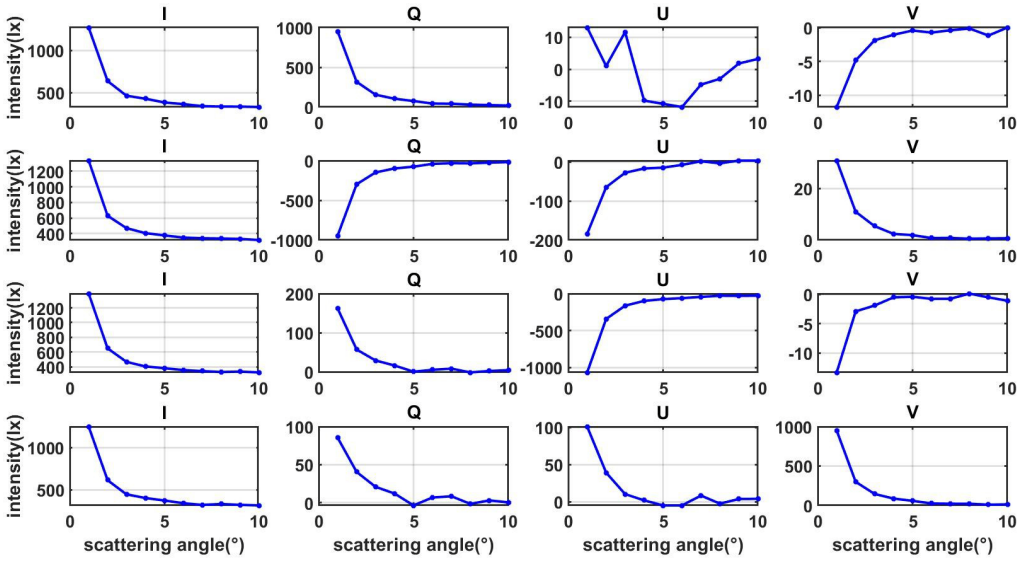

Fig. 9. Stokes vector of back-scattered light of dielectric surface (first row: p-light incident, second row: s-light incident, third row: 45° light incident, fourth row: right-hand circularly polarized light incident).

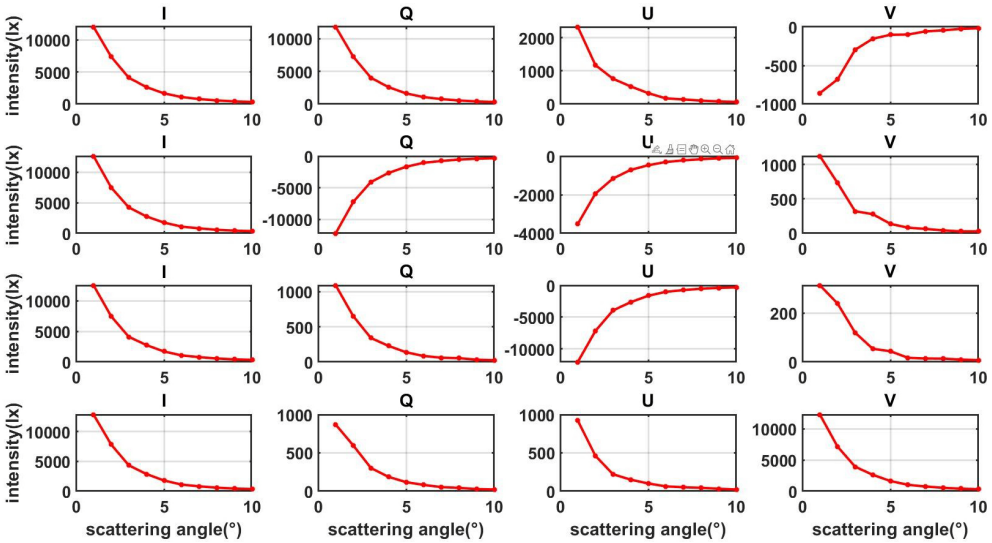

Fig. 10. Stokes vector of back-scattered light of metal surface (first row: p-light incident, second row: s-light incident, third row: 45° light incident, fourth row: right-hand circularly polarized light incident).

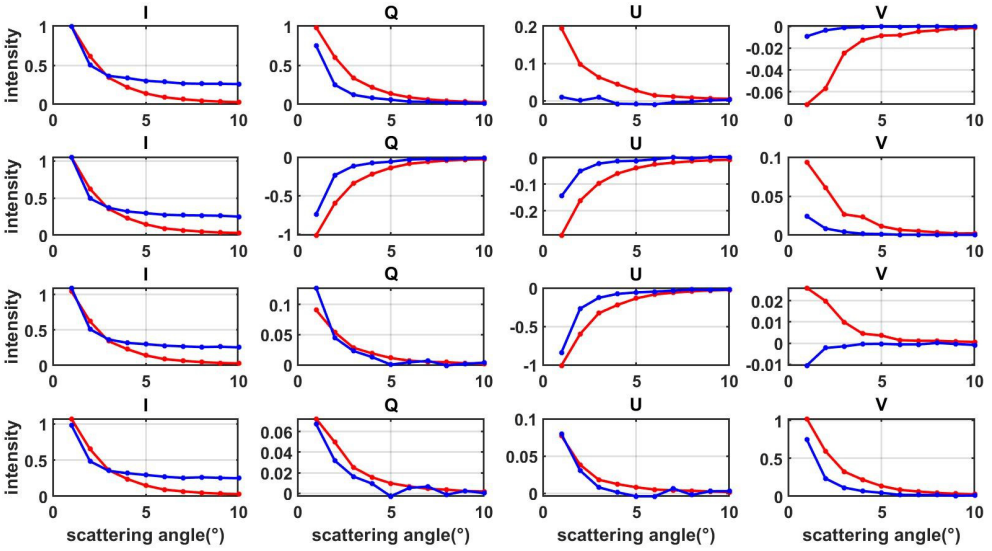

Fig. 11. Distribution of normalized Stokes vector (first row: p-light incident, second row: s-light incident, third row: 45° light incident, fourth row: right-hand circularly polarized light incident).

It can be seen that when p- and s-linearly polarized light is incident on metal rough surface, the scattered light exhibits obvious circular polarization component. When 45° linearly polarized light is incident on metal rough surface, the component of circular polarization of scattered light is very small. When p-, s-, and 45°-linearly polarized light is incident on dielectric rough surface, the component of circular polarization of

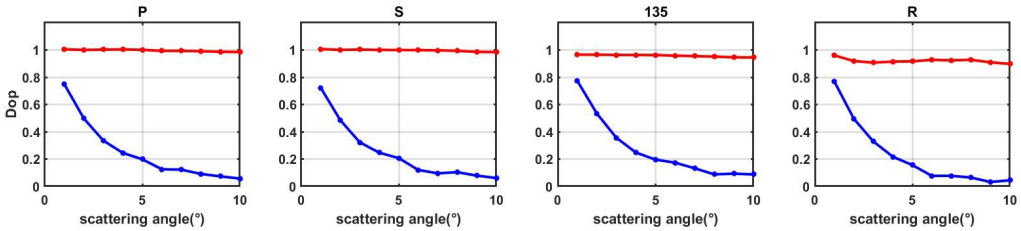

Fig. 12. Degree of polarization of back-scattered light of randomly rough surfaces (first row: p-light incident, second row: s-light incident, third row: 45° light incident, fourth row: right-hand circularly polarized light incident).

scattered light is very small. The fast axis direction of the wave plate and the transparent axis direction of the polarizer are not strictly calibrated by the manufacturer. Experimental errors should be taken into account. The experimental data are consistent with the numerical simulation results.

Figure 12 shows the degree of polarization (DOP) of back-scattered light of randomly rough surfaces. It can be seen that the metal rough surface has good polarization retention properties. With the increase of incident angle, the dielectric rough surface has good depolarization characteristics.

4.2.2. Mueller matrix of back-scattered light from metal rough surface

Figure 13 shows normalized Mueller matrix of back-scattered light of randomly rough surface. m_{11} represents the intensity of back-scattered light. As incident angle increas-

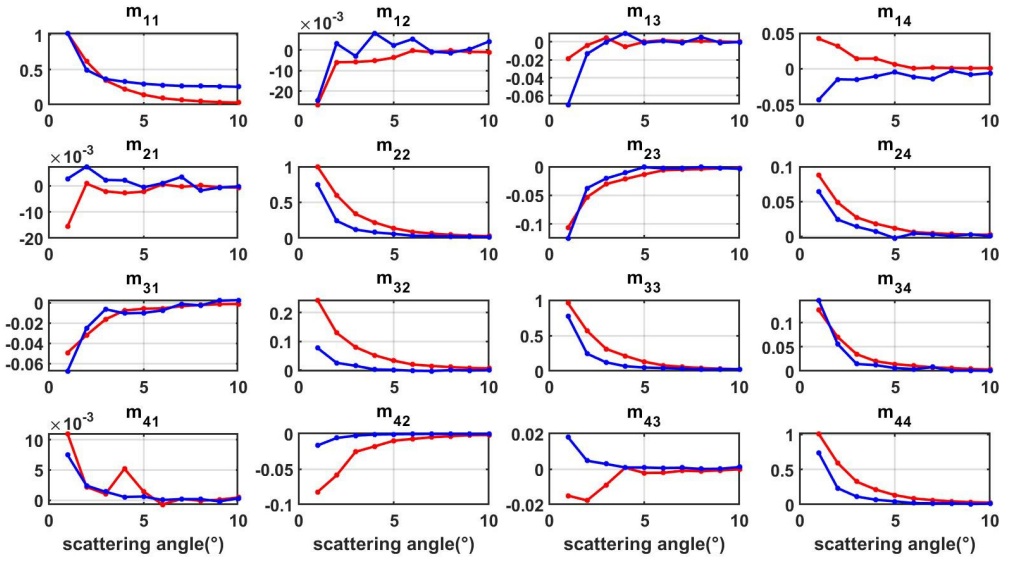

Fig. 13. Mueller matrix of back-scattered light of randomly rough surfaces (first row: p-light incident, second row: s-light incident, third row: 45° light incident, fourth row: right-hand circularly polarized light incident).

es, scattered light from metal rough surface decays to zero. The mirror image component of back-scattered light from metal surface is large. Back-scattered light from dielectric surfaces does not decay to zero. The diffuse component of back-scattered light from dielectric surface cannot be ignored, and there are great differences in m_{42} between metal and dielectric surfaces. The above research provides a new idea for laser detection and guidance device to identify metal targets.

5. Applications

Conventional lidar detects the position and speed of a target by calculating the flight time of the light beam. As the target material cannot be recognized, it is easily disturbed by the false targets. The polarization lidar considers both the intensity and polarization of the scattered light and improves the target recognition ability. The common polarized lidar structure is shown in Fig. 14. The laser is Nd:YAG polarized pulsed laser. The laser beam is expanded and collimated with a lens. The APD1 and APD2 can measure the vertical component $I(90°, 0)$ and horizontal component $I(0°, 0)$ of the intensity of the scattered light. In the $I(\alpha, \beta)$, α is the angle of polarization, and β stands for phase delay. We can calculate the depolarization of the scattered light P,

$$P = \frac{|I(90°, 0) - I(0°, 0)|}{|I(90°, 0) + I(0°, 0)|} \tag{27}$$

According to P, the target material can be judged [7].

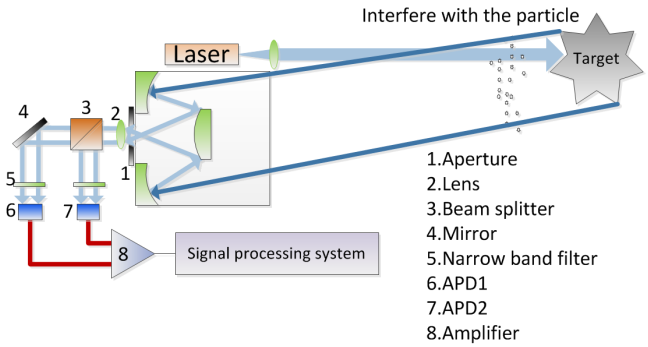

Fig. 14. The common polarized lidar structure.

Polarized lidar is better than ordinary radar in distinguishing target by the degree of depolarization of scattered light. However, when non-spherical particles are encountered in cirrus clouds, dust and haze, the degree of depolarization of the scattered light increases. The work of the polarization lidar is seriously interfered. We have designed a new polarization lidar. A circular polarization component detection channel is added to the polarization lidar. Its structure is shown in Fig. 15. We can measure $I(45°, \pi/2)$ when the angle between the fast axis of the quarter-wave plate and the polarizer is $\pi/2$.

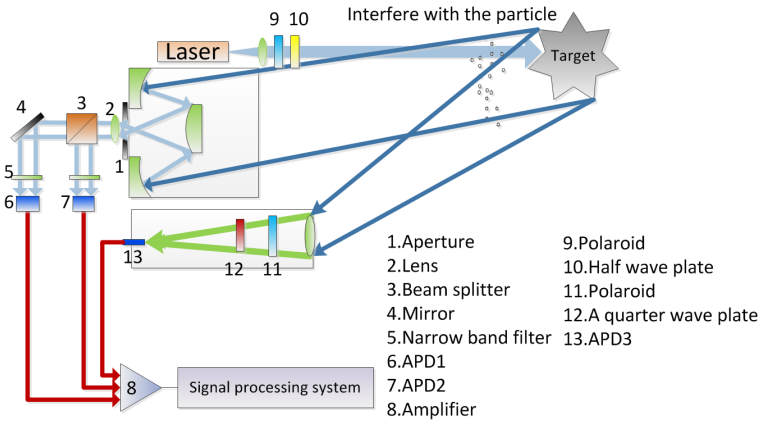

Fig. 15. The circularly polarized light component measurement channel.

During the detection, the stepper motor controls half of the wave plate rotation. Then the laser uses linearly polarized light with different polarization angle to illuminate the target. As the relative position of the target and lidar moves, the polarization angle changes constantly. We can calculate V by Eq. (26). When metal targets are detected, V has a peak distribution. V is always 0 for dielectric objects or atmospheric particles. By measuring the V, the polarization lidar can detect metal targets. V is only related to the material properties and has nothing to do with the target roughness, and the new polarization lidar has strong anti-interference ability.

Polarization imaging is an important method for target recognition [25–29]. Lidar is different from polarization imaging. Lidar is usually received by photodiode or avalanche photodiode. Sophisticated signal processing circuits can amplify or attenuate signal amplitude. So lidar is sensitive to light intensity and polarization information. Incidence angle and detection range have important influence on echo signal. However, the number of detection lines of lidar is small and the dimension of echo signal is low. CCD cameras are commonly used for polarization imaging. CCD is rarely used in lidar because they are highly integrated and prone to saturation. Polarization imaging can provide rich target image and polarization information, which is helpful to identify target features. Deep learning and convolutional neural network can be used to extract target features. Therefore, using polarization imaging technology to identify targets is an important research direction in the future.

6. Conclusion

In this paper, the Monte Carlo method is used to generate a large number of randomly rough surfaces to simulate target surfaces. Stokes vector of back-scattered light from metal and dielectric surfaces is numerically simulated using the Kirchhoff tangent plane approximation method with high precision. The results show that when s- and p-linearly polarized light is incident on a metal rough surface, there are obvious circular

polarization components in scattered light. When 45° linearly polarized light is incident on a metal rough surface, circular polarization component of scattered light is very small. A metal rough surface resembles a wave plate with phase delay. Fast axis of the wave plate is perpendicular or parallel to 45°. When linearly polarized light illuminates a dielectric rough surface, circular polarization component of back-scattered light is very small. Experimental data are consistent with the numerical results. A metal surface has good polarization preserving properties. With the increase of incident angle, dielectric surface has strong depolarization characteristics. The above research provides a new basis for laser detection and guidance system to identify metal targets.

Funding
This work was supported by the National Natural Science Foundation of China (NSFC) (61371167).

References

[1] Sanchez-Gil J.A., Nieto-Vesperinas M., Moreno F., Gonzalez F., *Speckle statistics of electromagnetic waves scattered from perfectly conducting random rough surfaces*, Journal of the Optical Society of America A **10**(12), 1993: 2628–2636, DOI: 10.1364/JOSAA.10.002628.

[2] Sánchez-Gil J.A., Nieto-Vesperinas M., *Resonance effects in multiple light scattering from statistically rough metallic surfaces*, Physical Review B **45**(15), 1992: 8623, DOI: 10.1103/PhysRevB.45.8623.

[3] Méndez E.R., Navarrete A.G., Luna R.E., *Statistics of the polarization properties of one-dimensional randomly rough surfaces*, Journal of the Optical Society of America A **12**(11), 1995: 2507–2516, DOI: 10.1364/JOSAA.12.002507.

[4] Izotova V.F., Maksimova I.L., Romanov S.V., *Simulation of polarization characteristics of the crystalline lens during protein aggregation with regard to multiple scattering*, Optics and Spectroscopy **86**, 1999: 902–908.

[5] Maksimova I.L., Romanov S.V., Izotova V.F., *The effect of multiple scattering in disperse media on polarization characteristics of scattered light*, Optics and Spectroscopy **92**(6), 2002: 915–923, DOI: 10.1134/1.1490031.

[6] Izotova V.F., Maksimova I.L., Romanov S.V., *Influence of shape and dimension of the cuvette on polarization characteristics of multiple scattered light*, Proc. SPIE **3726**, Saratov Fall Meeting '98: Light Scattering Technologies for Mechanics, Biomedicine, and Material Science, 1999: 370–380, DOI: 10.1117/12.341419.

[7] Wang S., Xu L., Li H., Xie S., *Monte Carlo simulation of the diffusely scattered polarized light in turbid media*, Proc. SPIE **5630**, Optics in Health Care and Biomedical Optics: Diagnostics and Treatment II, 2005: 823–832, DOI: 10.1117/12.576972.

[8] Jin L., Takizawa K., *Stokes parameters of reflected and scattered light by a rough surface*, Proc. SPIE **7432**, Optical Inspection and Metrology for Non-Optics Industries, 2009: 74320B, DOI: 10.1117/12.828030.

[9] Jin L., Yamaguchi K., Watanabe M., Hira S., Kondoh E., Gelloz B., *Polarization characteristics of scattered light from macroscopically rough surfaces*, Optical Review **22**, 2015: 511–520, DOI: 10.1007/s10043-015-0117-2.

[10] Delacrétaz Y., Seydoux O., Chamot S., Ettemeyer A., Depeursinge C., *Monte Carlo simulation of the field back-scattered from rough surfaces*, Journal of the Optical Society of America A **29**(3), 2012: 270–277, DOI: 10.1364/JOSAA.29.000270.

[11] Letnes P.A., Maradudin A.A., Nordam T., Simonsen I., *Calculation of all elements of the Mueller matrix for scattering of light from a two-dimensional randomly rough metal surface*, arXiv:1108.2599 [physics.optics].

[12] LETNES P.A., MARADUDIN A.A., NORDAM T., SIMONSEN I., *Calculation of the Mueller matrix for scattering of light from two-dimensional rough surfaces*, Physical Review A **86**(3), 2012: 031803(R), DOI: 10.1103/PhysRevA.86.031803.
[13] GUIRADO D., STAM D., *Monte Carlo and T-matrix modeling of the reflection of polarized light by rough, planetary surfaces*, European Planetary Science Congress 2012, IFEMA-Feria de Madrid, September 23–28, 2012, Madrid, Spain.
[14] GUIRADO D., STAM D.M., SMIT M., *A Monte Carlo model for the reflection of polarized light on surfaces*, 1st WG meeting, Warsaw, May 7–10, 2012.
[15] WANG C., GAO J., YAO T., WANG L., SUN Y., XIE Z., GUO Z., *Acquiring reflective polarization from arbitrary multi-layer surface based on Monte Carlo simulation*, Optics Express **24**(9), 2016: 9397–9411, DOI: 10.1364/OE.24.009397.
[16] GUAN F., ZHANG X., HAN H., ZHONG W., *Influence of size of the spherical scatterers and the attenuation coefficient on the polarization memory based on the Electric Monte Carlo simulation*, Proc. SPIE **10244**, International Conference on Optoelectronics and Microelectronics Technology and Application, 2017: 1024419, DOI: 10.1117/12.2266755.
[17] YUN T., ZENG N., LI W., LI D., JIANG X., MA H., *Monte Carlo simulation of polarized photon scattering in anisotropic media*, Optics Express **17**(19), 2009: 16590–16602, DOI: 10.1364/OE.17.016590.
[18] YUN T., LI W., JIANG X., MA H., *Monte Carlo simulation of polarized light scattering in tissues*, Journal of Innovative Optical Health Sciences **2**(2), 2009: 131–135, DOI: 10.1142/S1793545809000504.
[19] JIANG S., LAI J., WANG C., BIAN B., LU J., LI Z., *Describing the depolarization characteristic of rough surface by M11/M00 of Mueller matrix*, Proc. SPIE 7508, 2009 International Conference on Optical Instruments and Technology: Advanced Sensor Technologies and Applications, 2009: 75080R, DOI: 10.1117/12.836870.
[20] JIANG S., WANG C., LAI J., BIAN B., LU J., LI Z., *Monte Carlo simulation of Stokes vectors of polarized light scattering from two-dimensional random rough surfaces*, Journal of Modern Optics **58**(18), 2011: 1651–1658, DOI: 10.1080/09500340.2011.618278.
[21] YAN K., WANG S., JIANG S., XUE L., SONG Y., YAN Z., LI Z., *Calculation and analysis of Mueller matrix in light scattering detection*, Chinese Optics Letters **12**(9), 2014: 092901.
[22] YAN K., WANG S., JIANG S., SONG Y., XUE L., YAN Z., LI Z., *Full angular Stokes vectors of light scattering from two-dimensional randomly rough surfaces by Kirchhoff approximation method*, Journal of Optics **16**(10), 2014: 105714, DOI: 10.1088/2040-8978/16/10/105714.
[23] WANG S., XUE L., YAN K., *Numerical calculation of light scattering from metal and dielectric randomly rough Gaussian surfaces using microfacet slope probability density function based method*, Journal of Quantitative Spectroscopy and Radiative Transfer **196**, 2017: 183–200, DOI: 10.1016/j.jqsrt.2017.04.016.
[24] YAN K., YANG S., ZHAO Y., MA C., JIN Y., WANG S., *Deep learning for light scattering computation: Reconstructing light scattering fields from 1-D randomly rough surfaces as an example*, Computer Physics Communications **270**, 2022: 108183, DOI: 10.1016/j.cpc.2021.108183.
[25] WANG X., HU T., LI D., GUO K., GAO J., GUO Z., *Performances of polarization-retrieve imaging in stratified dispersion media*, Remote Sensing **12**(18), 2020: 2895, DOI: 10.3390/rs12182895.
[26] LI D., XU C., ZHANG M., WANG X., GUO K., SUN Y., GAO J., GUO Z., *Measuring glucose concentration in a solution based on the indices of polarimetric purity*, Biomedical Optics Express **12**(4), 2021: 2447–2459, DOI: 10.1364/BOE.414850.
[27] LI D., GUO K., SUN Y., BI X., GAO J., GUO Z., *Depolarization characteristics of different reflective interfaces indicated by indices of polarimetric purity (IPPs)*, Sensors **21**(4), 2021: 1221, DOI: 10.3390/s21041221.
[28] LI D., XU C., YAN L., GUO Z., *High-performance scanning-mode polarization based computational ghost imaging (SPCGI)*, Optics Express **30**(11), 2022: 17909–17921, DOI: 10.1364/OE.458487.
[29] LI D., LIN B., WANG X., GUO Z., *High-performance polarization remote sensing with the modified U-Net based deep-learning network*, IEEE Transactions on Geoscience and Remote Sensing **60**, 2022: 5621110, DOI: 10.1109/TGRS.2022.3164917.

[30] Toporkov J.V., *Study of Electromagnetic Scattering from Randomly Rough Ocean-Like Surfaces Using Integral-Equation-Based Numerical Technique*, PhD Thesis, Virginia Polytechnic Institute and State University, 1998.
[31] Tsang L., Kong J.A., Ding K.H., Ao C.O., *Scattering of Electromagnetic Waves: Numerical Simulations*, Wiley, 2001.
[32] Wu J.J., *Simulation of rough surfaces with FFT*, Tribology International **33**(1), 2000: 47–58, DOI: 10.1016/S0301-679X(00)00016-5.
[33] Jiang Y., Li Z., *Monte Carlo simulation of Mueller matrix of randomly rough surfaces*, Optics Communications **474**, 2020: 126113, DOI: 10.1016/j.optcom.2020.126113.
[34] Sanchez-Gil J.A., Nieto-Vesperinas M., *Light scattering from random rough dielectric surfaces*, Journal of the Optical Society of America A **8**(8), 1991: 1270–1286, DOI: 10.1364/JOSAA.8.001270.
[35] Knotts M.E., O'Donnell K.A., *Measurements of light scattering by a series of conducting surfaces with one-dimensional roughness*, Journal of the Optical Society of America A **11**(2), 1994: 697–710, DOI: 10.1364/JOSAA.11.000697.
[36] Chaikina E.I., Negrete-Regagnon P., Ruiz-Cortés V., Méndez E.R., *Measurements of the hemispherical scattering distribution function of rough dielectric surfaces*, Optics Communications **208**(4–6), 2002: 215–221, DOI: 10.1016/S0030-4018(02)01581-X.
[37] Caron J., Lafait J., Andraud C., *Catastrophe theory interpretation of multiple peaks produced by light scattering from very rough dielectric surfaces*, Physica B: Condensed Matter **325**, 2003: 76–85, DOI: 10.1016/S0921-4526(02)01452-7.
[38] Jiang Y., Li Z., *Mueller matrix of laser scattering by a two-dimensional randomly rough surface*, Journal of Quantitative Spectroscopy and Radiative Transfer **287**, 2022: 108225, DOI: 10.1016/j.jqsrt.2022.108225.
[39] Schaefer B., Collett E., Smyth R., Barrett D., Fraher B., *Measuring the Stokes polarization parameters*, American Journal of Physics **75**(2), 2007: 163–168, DOI: 10.1119/1.2386162.

Received March 4, 2022
in revised form June 12, 2022